Computer Modeling in Engineering & Sciences

Tech Science Press

https://doi.org/10.32604/cmes.2026.084395

ARTICLE

Contact Force Tracking in Robotics Using Reference-Dependent Constant Impedance Control

Abubaker Ahmed[1], **Hosham Wahballa**[2,*], **AlaEldin Awouda**[3], **Arafat Abdulgader Mohammed Elhag**[4], **Ahmed Hamza Osman**[5] **and Mubarak Himmat**[6]

[1]School of Automation Engineering, Wuxi University, Wuxi, 214000, China
[2]School of Mechanical and Electrical Engineering, Quanzhou University of Information Engineering, Fujian, 362000, China
[3]Mechanical Engineering Department, College of Engineering, University of Bisha, Bisha, Saudi Arabia
[4]Department of Computer and Information System, Bisha Applied College, University of Bisha, Bisha, Saudi Arabia
[5]Department of Information Systems, Faculty of Computing and Information Technology in Rabigh, King Abdulaziz University, Jeddah, 21911, Saudi Arabia
[6]Horizon University College, School of Computing, Emirate of Ajman, United Arab Emirates

*Corresponding Author: Hosham Wahballa. Email: hosham@qzuie.edu.cn

Received: 21 April 2026; Accepted: 11 August 2026; Published: 28 August 2026

ABSTRACT: Accurate force regulation is essential in robotic contact tasks such as polishing, grinding, and assembly. However, conventional impedance controllers often exhibit limited force-tracking accuracy, while adaptive methods require high tuning effort and computational cost. To address these issues, this paper proposes a Constant Impedance Force Controller (CIFC) based on a Force Reference Dependent Impedance (F_{RDI}) model, which is developed and validated through computer modeling and simulation. Robot environment interaction is computationally modeled as a mass damper spring system, and a position-based impedance framework is employed to regulate force deviations. A compensation signal derived from the F_{RDI} stiffness and damping terms reduces tracking errors while preserving constant impedance characteristics. Stability is proven using Lyapunov analysis. Numerical simulations and experimental validation demonstrate that the proposed method achieves robust force tracking under multi-source uncertainties on ramp, curved, and complex surfaces. The CIFC achieves an average force-tracking RMS error of 0.15 N in simulation, compared with 0.11–0.19 N for the benchmark methods. Experimentally, RMS errors range from 0.24 to 0.52 N under reference forces of 5–15 N on curved and complex surfaces, with maximum deviations of ±0.35 and ±0.50 N, respectively. These results confirm the effectiveness of the proposed modeling and simulation framework, demonstrating improved robustness and tracking consistency over conventional impedance control.

KEYWORDS: CIFC method; force tracking; force corrector; polishing process; complex surfaces

1 Introduction

Impedance control has become a foundational strategy in robotic interaction control since it was introduced by Hogan in 1985 [1,2]. It enables the dynamic regulation of interactions between a robot and its environment by modulating virtual parameters such as inertia, damping, and stiffness [3,4]. Unlike traditional position or force control methods, impedance control inherently supports compliant interactions, facilitating safe and adaptive physical contact in dynamic or uncertain environments [5].

In dynamic robotic environments, control complexity increases as systems must continuously adapt to unpredictable conditions [6]. Although conventional single impedance controllers perform effectively in controlling force on surfaces with known characteristics [7,8], they face significant limitations when robots interact with complex or irregular geometries [9]. These shortcomings are particularly critical in precision contact tasks that demand adaptive and responsive physical interaction. To address these challenges, many researchers have developed advanced control strategies to enhance force tracking performance.

Simple impedance control is an effective strategy for force tracking in known environments due to its fixed stiffness, damping, and inertia parameters [6,10,11]. However, it often underperforms in uncertain or dynamic environments, where its inability to adapt to varying contact conditions can lead to unstable interactions, excessive contact forces, or poor tracking accuracy [12–14]. To address these limitations, enhanced variable strategies such as adaptive impedance control [5,15,16], hybrid force impedance schemes [9,17], neural network (NN)-based approaches [18,19], and learning-based techniques [20,21] have been developed. These methods allow real-time adjustment of impedance parameters, significantly improving robustness and adaptability in complex and unpredictable environments.

This paper develops a compensated impedance control framework for accurate contact force tracking, where the impedance parameters (m_r, b_r, and k_r) remain fixed throughout the control process. In contrast to existing control methods that mainly regulate interaction behavior through impedance parameters or variable impedance adjustment, the proposed CIFC framework introduces a Force Reference Dependent Impedance (F_{RDI}) mechanism to enhance force regulation performance. The F_{RDI} term is formulated according to the desired interaction force and contact conditions, providing an additional compensation channel to reduce force tracking errors during robot environment interaction. Different from traditional feedforward compensation methods that mainly compensate unknown robot dynamics or trajectory-related effects, the proposed mechanism directly addresses interaction force deviations based F_{RDI} mechanism, while using fixed impedance parameters. Therefore, CIFC improves force tracking accuracy and adaptability to curved and complex surfaces without increasing controller complexity. With respect to previous works, the key contributions of this paper are as follows:

1. A compensated impedance control framework is proposed for robotic contact tasks, where the impedance parameters (m_r, b_r and k_r) remain fixed throughout the control process. Unlike methods relying on online impedance parameter adjustment, the proposed approach improves position and force tracking-based compensation concept.
2. The F_{RDI} mechanism is introduced to enhance conventional impedance control. The proposed compensation term is generated according to the desired interaction force and contact conditions, reducing force tracking errors and improving adaptability during robot environment interaction.
3. The proposed force and position control framework is experimentally validated through polishing-like contact tasks. The results demonstrate reliable contact force regulation and accurate motion tracking on curved and complex surfaces, showing its potential for applications such as polishing, grinding, and other contact-based manufacturing processes.

The structure of this paper is organized as follows: Section 3 introduces the dynamic modeling and control framework. Section 4 presents the simulation results and comparative analysis. Section 5 describes the experimental validation. Finally, concluding remarks are provided in Section 6.

2 Related Works

Significant research efforts have been devoted to enhancing force and position tracking by improving classical impedance control through various advanced strategies.

Duan et al. [5] proposed an adaptive impedance control method that updates impedance parameters online to improve force regulation under uncertain contact conditions. Jung et al. [8] developed an adaptive impedance framework for dynamic environments and demonstrated improved force tracking accuracy compared with fixed parameter impedance control through both simulation and experimental validation. Wang et al. [12] introduced a PD-enhanced adaptive impedance strategy for robotic grinding and polishing, which reduced force tracking error, improved overall performance, and minimized overshoot.

Shahriari et al. [22] proposed a decentralized control strategy for multi-robot manipulation of large objects, addressing limitations of conventional coupled impedance and hybrid force/position control methods. Experimental results using a dual-arm system confirmed improved coordinated manipulation performance.

For hybrid impedance control, Cao et al. [9] designed a hybrid PID-adaptive impedance controller that reduces force overshoot and tracking error, with validation across free motion, impact, and sustained contact conditions. Recently, Saat et al. [23] proposed a BELBIC-PID controller for flexible joint manipulators, integrating brain emotional learning with PID control to improve trajectory tracking performance. The results demonstrated enhanced tracking accuracy and robustness against disturbances compared with conventional PID-based controllers. Furthermore, Nasir et al. [24] proposed a hybrid spiral bacterial foraging optimization algorithm to tune a fuzzy logic controller for flexible manipulators. The results demonstrated improved convergence speed, tracking accuracy, and hub-angle regulation compared with conventional optimization approaches. Furthermore, Ghazali et al. [25] proposed a neuroendocrine-PID controller optimized using an adaptive safe experimentation dynamics algorithm, achieving stable convergence and improved tracking performance for nonlinear systems. Ajani and Assal [26] developed an autonomous robotic tooth brushing system using hybrid impedance control combined with vision-based head pose estimation to adapt brushing trajectories in real time. Jung and Lee [27] integrated hybrid force control with impedance reduction and time-delay compensation, improving contact stability and force tracking in a multi-link robotic system.

In neural network-based impedance control, Li et al. [28] proposed a finite-time NN-based impedance controller with barrier Lyapunov functions and disturbance observers to ensure fast convergence and constraint satisfaction under uncertainties. Hasanzadeh et al. [29] developed a dual-loop NN-impedance controller for rehabilitation robots, where a wavelet neural network generates motion trajectories and an adaptive impedance layer ensures accurate force and position tracking. Peng et al. [19] introduced an adaptive NN-based impedance control scheme for electrically driven robots with unmeasured states, where neural observers estimate system variables to maintain stability under uncertainty.

Finally, in learning-based impedance control, Roveda et al. [30] proposed a real-time reinforcement learning framework for impedance adaptation in human-robot interaction tasks, demonstrating improved performance in experimental lifting operations. Sharifi et al. [21] developed a learning-based adaptive impedance controller that adjusts robot behavior online without force sensing, with stability guaranteed via Lyapunov analysis and validated through real-time experiments.

Despite significant improvements in adaptability achieved by advanced impedance control strategies, including adaptive, hybrid, and learning-based approaches, these methods still introduce additional complexity in practical robotic contact tasks. In particular, they often require online adjustment of impedance parameters, prior training data, or increased computational resources, which may limit their real-time applicability and ease of deployment in industrial environments. In contrast, this work aims to address these limitations by maintaining constant impedance parameters while introducing an additional force reference-dependent compensation mechanism to enhance force tracking performance. This formulation preserves the simplicity of classical impedance control while improving its effectiveness in curved and complex surface interaction tasks.

3 Dynamic and Control System

This section covers both the dynamic impedance controller and the proposed CIFC method.

Firstly, the dynamic model of an n-DOF robotic manipulator in joint space can generally be formulated as follows:

$$M(q)\ddot{q} + C(q,\dot{q})\dot{q} + G(q) + \sigma_f(\dot{q}) = \tau_d - \tau_e \tag{1}$$

where $M(q)$ is the symmetric positive definite inertia matrix; q, $\dot{q}$ and $\ddot{q}$ denote the joint position, velocity, and acceleration vectors, respectively; $C(q,\dot{q})$ represents the Coriolis and centrifugal torques; $G(q)$ is the gravity torque vector; σ_f is the friction torque vector; τ_d is the motor control input torque; and τ_e is the external disturbance torque. The transformation from joint coordinate to Cartesian coordinate is expressed as:

$$\dot{x} = J(q)\dot{q} \tag{2}$$

where $J(q)$ is a Jacobian matrix and $\dot{x}$ is Cartesian velocity; by taking the derivative of Eq. (2) we can get:

$$\ddot{x} = J(q)\ddot{q} + \dot{J}(q)\dot{q} \tag{3}$$

where $\ddot{x}$ is Cartesian acceleration; rewrite Eq. (3) as:

$$\ddot{q} = (J(q))^{-1}(\ddot{x} - \dot{J}(q)\dot{q}) \tag{4}$$

By substituting Eq. (4) in Eq. (1) yield:

$$\begin{aligned} &M(q)(J(q))^{-1}(\ddot{x} - \dot{J}(q)\dot{q}) + C(q,\dot{q})\dot{q} + G(q) \\ &\quad + \sigma_f(\dot{q}) = \tau_d - \tau_e \end{aligned} \tag{5}$$

The desired force torque interaction is formally expressed as, $[\tau_d = (J(q))^T f_d]$ then, by multiplying both sides of Eq. (5) by $(J(q))^{-T}$ yield:

$$\begin{aligned} &(J(q))^{-T}M(q)(J(q))^{-1}\ddot{x} - (J(q))^{-T}M(q)(J(q))^{-1}\dot{J}(q)\dot{q} \\ &\quad + (J(q))^{-T}C(q,\dot{q})\dot{q} + (J(q))^{-T}G(q) + (J(q))^{-T}\sigma_f(\dot{q}) \\ &\quad = (J(q))^{-T}\tau_d - (J(q))^{-T}\tau_e \end{aligned} \tag{6}$$

Remark 1: *The transformation from joint space dynamics to Cartesian space dynamics assumes that the manipulator Jacobian J(q) is full rank and invertible. This assumption is satisfied for the 6-DOF UR10 manipulator used in this study because all contact trajectories (for polishing and similar) are planned within a workspace that avoids singular configurations. Consequently, J^{-1} and J^{-T} exist throughout the experiments. For redundant manipulators or motions near singularities, pseudoinverse-based and singularity-robust formulations should be adopted, which are outside the scope of the present work.*

Eq. (6) can be rewritten as:

$$\hat{M}\ddot{x} + \hat{u} + \hat{G} + f_{\hat{f}} = f_d - f_e \tag{7}$$

where,

$$\hat{M} = \frac{M(q)}{J(q)^T J(q)};\ \hat{u} = \frac{C(q,\dot{q})\dot{q}}{(J(q))^T} - M(q)\frac{\dot{J}(q)}{(J(q))^T J(q)}\dot{q};\ \hat{G} = \frac{G(q)}{(J(q))^T};\ f_{\hat{f}} = \frac{\sigma_f(\dot{q})}{(J(q))^T};\ f_d = \frac{\tau_d}{(J(q))^T};\ f_e = \frac{\tau_e}{(J(q))^T}$$

in which, $\hat{M}$ is the estimated inertia matrix in Cartesian space, $\hat{u}$ is estimated of coriolis and centrifugal torques, $\hat{G}$ is an estimated gravity torque, $f_{\hat{f}}$ is an estimated Cartesian space friction force, f_d is desired input force, and f_e is an external force.

To simplify the Cartesian space dynamics for low-speed robotic contact tasks, the following assumptions are introduced:

Assumption 1: *Bounded residual dynamics:*

For low-speed contact tasks such as continuous contact operations (polishing, grinding, debburing, etc.), the nonlinear dynamics (Coriolis, gravity, and friction) are assumed to be partially compensated by the inner loop controller. The remaining effect is modeled as a bounded residual term:

$$\hat{u} + \hat{G} + f_{\hat{f}} \approx \Delta, \quad \|\Delta\| \le \varepsilon \tag{8}$$

Substituting into Eq. (7) gives:

$$\hat{M}\ddot{x} + \Delta \approx f_d - f_e \tag{9}$$

During stable contact, the residual dynamics are much smaller than the interaction force variation:

$$\|\Delta\| \ll \|f_d - f_e\| \tag{10}$$

Assumption 2: *Quasi-static contact condition:*

Under quasi-static conditions ($\ddot{x} \approx 0$) and effective compensation ($\Delta \approx 0$), Eq. (9) reduces to:

$$f_d \approx f_e \tag{11}$$

Force tracking error form became:

$$\delta f = f_e - f_d \approx 0 \tag{12}$$

The above dynamic model employed in this work is the classical rigid body manipulator model widely used in robot control literature. The formulation follows the standard Euler-Lagrange representation of robotic dynamics and serves as the theoretical basis for the subsequent Cartesian space force control development [10,11,31]. The proposed CIFC controller is experimentally validated on a UR10 robotic manipulator to verify the effectiveness of the model-based control framework. Fig. 1 presents the UR10 manipulator and the dynamic modeling procedure used in this work, where the conventional joint space robot dynamics are transformed into a Cartesian space force control model through Jacobian based coordinate transformation and subsequent simplification under contact task assumptions.

3.1 Proposed Constant Impedance Force Controller (CIFC)

Mechanical impedance defines the relationship between a velocity (input) and a resulting contact force (output) at its interaction with the environment. Accordingly, in the Laplace transform framework, the impedance $z(s)$ is expressed as the ratio between a force deviation $\delta f(s)$ and the corresponding velocity error $\dot{e}(s)$:

$$\delta f(s) = z(s)\dot{e}(s) \tag{13}$$

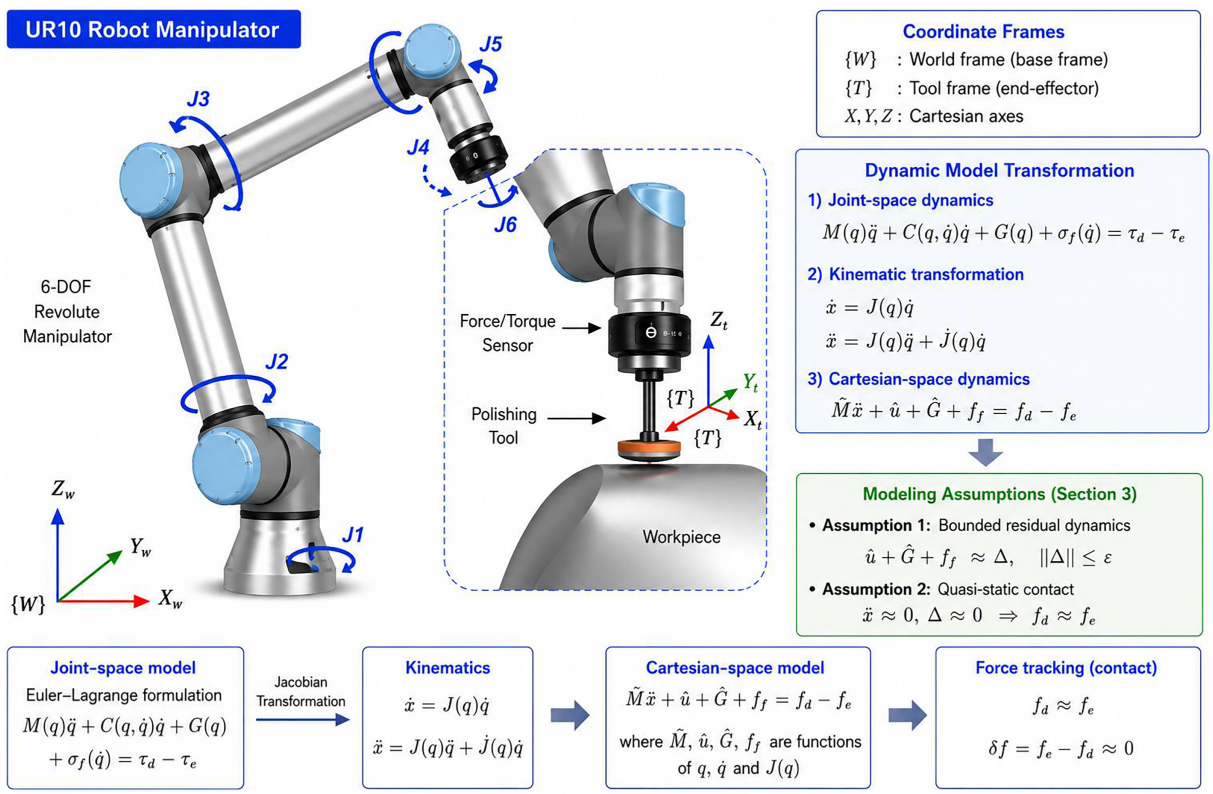

Figure 1: The UR10 manipulator model is transformed from joint space dynamics to a Cartesian space force control formulation using Jacobian-based coordinate transformation and contact task assumptions.

Then rewrite Eq. (13) as:

$$\delta f(s) = sz(s)e(s) \tag{14}$$

Typically, in robotics, the impedance $z(s)$ is represented as:

$$z(s) = m_r s + b_r + k_r/s \tag{15}$$

where m_r, b_r, and k_r represent the robot's mass, damper, and stiffness parameters, respectively. The position error $e(s)$ corresponds to the difference between the current position $x(a)$ and the desired position $x(d)$, formulated as:

$$e(s) = x_a(s) - x_d(s) \tag{16}$$

Replacing Eqs. (16) and (15) into Eq. (14) leads to:

$$\delta f(s) = (m_r s^2 + b_r s + k_r)\cdot(x_a(s) - x_d(s)) \tag{17}$$

For simplicity, a one-dimensional interaction force is considered in the subsequent analysis. After performing the inverse Laplace transform and restructuring Eq. (17), the resulting time-domain representation of the impedance is:

$$\delta f = m_r(\ddot{x}_a - \ddot{x}_d) + b_r(\dot{x}_a - \dot{x}_d) + k_r(x_a - x_d) \tag{18}$$

The external force f_e presents within δf in Eq. (8) is typically modeled as a virtual spring characterized by a constant stiffness k_e. If the manipulator remains in contact with the environment, the corresponding external force f_e is given by:

$$f_e = k_e(x_e - x_a) \tag{19}$$

where k_e is environment stiffness, x_e is an external position, and x_a is an actual position.

Fig. 2 depicts the robot environment interaction, where the robot is modeled as an MDS system characterized by parameters (m_r, b_r, k_r), and the environment is simplified as a single spring element. A schematic overview of the proposed CIFC framework is presented in Fig. 3.

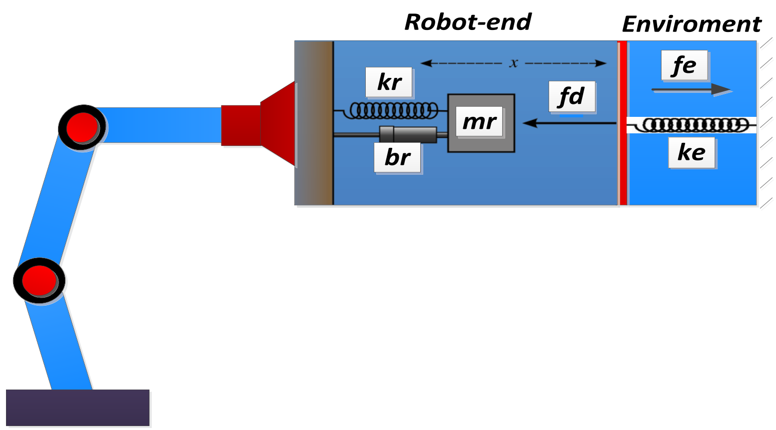

Figure 2: Robotic environment contact model in MDS system.

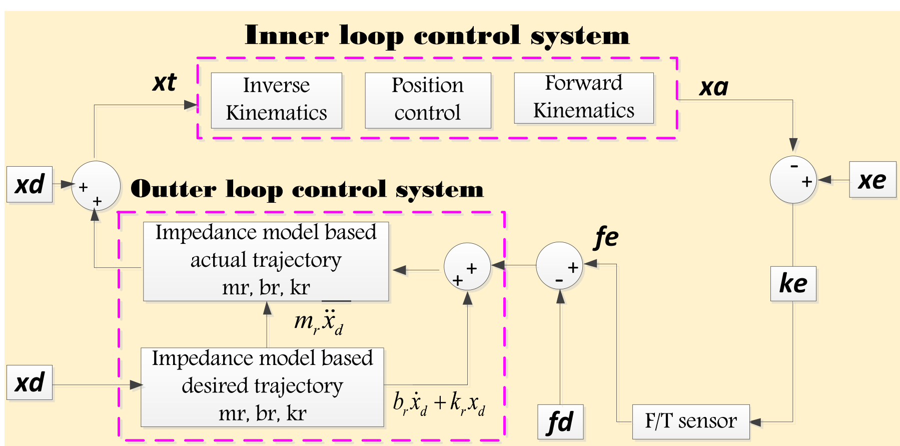

Figure 3: Schematic diagram of the CIFC controller based on a reference-dependent impedance model.

The Eqs. (18) and (19) describe a single impedance control scheme, meaning that no techniques are employed to adjust the impedance parameters in order to achieve specific performance. While this control strategy provides a basic framework for contact dynamics, a key limitation lies in its inability to maintain accurate contact force, especially when interacting with complex or uncertain environments. This challenge becomes more pronounced as the environment conditions vary or become nonlinear. To address this issue, numerous researchers have focused on tuning the impedance parameters, particularly the damping coefficient b_r and environment stiffness k_e. Various approaches have been proposed over the past two decades, including adaptive control, neural networks, and learning techniques, to enhance force tracking and system adaptability under variable contact conditions.

This paper presents a compensated impedance control strategy to improve contact force tracking while maintaining constant impedance parameters. Based on the impedance relationship, the force tracking error can be expressed as:

$$\delta f = (m_r\ddot{x}_a + b_r\dot{x}_a + k_r x_a) - (m_r\ddot{x}_d + b_r\dot{x}_d + k_r x_d) \tag{20}$$

where the second term represents the complete reference-dependent impedance response generated from the desired trajectory. It describes the expected interaction behavior under the predefined impedance parameters, including the inertial, damping, and stiffness effects.

Accordingly, the complete reference-dependent impedance force can be defined as:

$$F^{*}_{RDI} = m_r\ddot{x}_d + b_r\dot{x}_d + k_r x_d \tag{21}$$

For robotic contact tasks such as polishing and similar, the interaction process is generally performed under low-speed and smooth motion conditions. In this case, the desired acceleration $\ddot{x}_d$ remains relatively small compared with the velocity and position-dependent components. Moreover, the acceleration term is mainly related to transient motion changes, while the desired velocity and position terms directly represent the continuous contact behavior and the required interaction force.

Therefore, the compensation term used in this work is obtained by retaining the dominant damping and stiffness components:

$$F_{RDI} = b_r\dot{x}_d + k_r x_d \tag{22}$$

The proposed F_{RDI} term therefore represents a simplified reference-dependent compensation force that captures the main desired contact behavior and provides an additional force regulation mechanism within the impedance control framework. This formulation reduces force tracking errors while avoiding unnecessary computational complexity associated with acceleration estimation.

By rearranging Eq. (20) and combining it with Eq. (22), we obtain:

$$\Delta f_{CIFC} = \delta f + F_{RDI} = m_r(\ddot{x}_a - \ddot{x}_d) + b_r\dot{x}_a + k_r x_a \tag{23}$$

Rearranging for $\ddot{x}_a$:

$$m_r(\ddot{x}_a - \ddot{x}_d) = \Delta f_{CIFC} - b_r\dot{x}_a - k_r x_a \tag{24}$$

$$\ddot{x}_a - \ddot{x}_d = \frac{1}{m_r}(\Delta f_{CIFC} - b_r\dot{x}_a - k_r x_a) \tag{25}$$

$$\ddot{x}_a = \ddot{x}_d + \frac{1}{m_r}(\Delta f_{CIFC} - b_r\dot{x}_a - k_r x_a) \tag{26}$$

Therefore, Eq. (27) should be written as:

$$\ddot{x}_a = \ddot{x}_d + \frac{1}{m_r}(\Delta f_{CIFC} - b_r\dot{x}_a - k_r x_a) \tag{27}$$

and

$$\begin{cases} \dot{x}_a(t) = \dot{x}_a(t-1) + \ddot{x}_a(t) \cdot T \\ x_a(t) = x_a(t-1) + \dot{x}_a(t) \cdot T \end{cases} \tag{28}$$

where Δf_{CIFC} denotes the force error after applying the reconfigured compensation signal F_{RDI} to the controller model; and where T is the sample time between the controller and servo system.

3.2 Stability Analysis

The stability of the proposed CIFC controller is analyzed using Lyapunov theory. The derivation is conducted based on a reduced-order second-order impedance dynamics model that captures the dominant interaction behavior between the robot and the environment. From the CIFC interaction model in Eq. (23), we have:

$$\Delta f_{CIFC} = \delta f + F_{RDI} \tag{29}$$

where:

$$\delta f = f_e - f_d \tag{30}$$

and:

$$F_{RDI} = m_r(\ddot{x}_a - \ddot{x}_d) + b_r\dot{x}_a + k_r x_a \tag{31}$$

Define the tracking error:

$$e_x = x_a - x_d \tag{32}$$

$$\dot{e}_x = \dot{x}_a - \dot{x}_d \tag{33}$$

$$\ddot{e}_x = \ddot{x}_a - \ddot{x}_d \tag{34}$$

Substituting Eqs. (32)–(34) into Eq. (31) gives:

$$F_{RDI} = m_r\ddot{e}_x + b_r\dot{e}_x + k_r e_x + b_r\dot{x}_d + k_r x_d \tag{35}$$

Thus, the interaction dynamics become:

$$\Delta f_{CIFC} = m_r\ddot{e}_x + b_r\dot{e}_x + k_r e_x + d(t) \tag{36}$$

where:

$$d(t) = (f_e - f_d) + b_r\dot{x}_d + k_r x_d \tag{37}$$

Rearranging Eq. (38) yields:

$$m_r\ddot{e}_x + b_r\dot{e}_x + k_r e_x = \Delta f_{CIFC} - d(t) \tag{38}$$

Define the control input:

$$u(t) = \Delta f_{CIFC} \tag{39}$$

Then:

$$m_r \ddot{e}_x + b_r \dot{e}_x + k_r e_x = u(t) - d(t) \tag{40}$$

3.2.1 State-Space Representation

Define the state variables:

$$x_1 = e_x, \quad x_2 = \dot{e}_x \tag{41}$$

Then:

$$\dot{x}_1 = x_2 \tag{42}$$

$$\dot{x}_2 = -\frac{k_r}{m_r}x_1 - \frac{b_r}{m_r}x_2 + \frac{1}{m_r}u(t) - \frac{1}{m_r}d(t) \tag{43}$$

This can be written as:

$$\dot{x} = Ax + Bu + Bw \tag{44}$$

where:

$$w(t) = -d(t) \tag{45}$$

3.2.2 Assumption (Physical Boundedness)

In practical robotic contact tasks, the following physical constraints hold:

$$|x_d| \le X_{\max}, \quad |\dot{x}_d| \le V_{\max}, \quad |f_e - f_d| \le F_{\max} \tag{46}$$

Thus:

$$|d(t)| \le d_{\max} \tag{47}$$

where:

$$d_{\max} = F_{\max} + b_r V_{\max} + k_r X_{\max} \tag{48}$$

3.2.3 Lyapunov Function

Consider the quadratic Lyapunov function:

$$V = \frac{1}{2}k_r x_1^2 + \frac{1}{2}m_r x_2^2 \tag{49}$$

Since $m_r > 0$ and $k_r > 0$, V is positive definite and radially unbounded. The time derivative is:

$$\dot{V} = k_r x_1 \dot{x}_1 + m_r x_2 \dot{x}_2 \tag{50}$$

Substituting system dynamics:

$$\dot{V} = k_r x_1 x_2 + m_r x_2 \left(-\frac{k_r}{m_r}x_1 - \frac{b_r}{m_r}x_2 + \frac{1}{m_r}u(t) - \frac{1}{m_r}d(t)\right) \tag{51}$$

Simplifying:

$$\dot{V} = -b_r x_2^2 + x_2 u(t) - x_2 d(t) \tag{52}$$

3.2.4 Bounding the Input Terms

Applying Young's inequality:

$$|x_2 u(t)| \leq \frac{b_r}{4} x_2^2 + \frac{1}{b_r} u(t)^2 \tag{53}$$

$$|x_2 d(t)| \leq \frac{b_r}{4} x_2^2 + \frac{1}{b_r} d(t)^2 \tag{54}$$

Thus:

$$\dot{V} \leq -\frac{b_r}{2} x_2^2 + \frac{1}{b_r} \left(u(t)^2 + d(t)^2 \right) \tag{55}$$

3.2.5 Stability Result

Since both $u(t)$ and $d(t)$ are bounded in practical implementation, there exist constants $u_{\max}$ and $d_{\max}$ such that:

$$\dot{V} \leq -\frac{b_r}{2} x_2^2 + \frac{1}{b_r} (u_{\max}^2 + d_{\max}^2) \tag{56}$$

This inequality implies that the closed-loop system is:

- Input-to-State Stable (ISS)
- Uniformly Ultimately Bounded (UUB)

Therefore, the tracking error satisfies:

$$\limsup_{t \to \infty} \| e_x(t) \| \leq \epsilon \tag{57}$$

where ϵ depends on $u_{\max}$, $d_{\max}$, and controller parameters.

Since the force tracking error is given by $f_e - f_d = m_r \ddot{e}_x + b_r \dot{e}_x + k_r e_x$, and the closed-loop analysis ensures that e_x, $\dot{e}_x$, and $\ddot{e}_x$ are uniformly ultimately bounded, it follows that the force tracking error is also uniformly ultimately bounded. Therefore, the proposed CIFC framework guarantees bounded force tracking performance, where the steady state error depends on system parameters and disturbance magnitude.

It should be emphasized that the presented Lyapunov analysis is conducted on a reduced-order contact-level model to capture the dominant force-motion interaction behavior. A complete nonlinear multi-DOF stability proof, including full robot dynamics, coupling effects, and uncertainties, is beyond the scope of this work and is typically treated separately in impedance-based contact control literature due to its analytical complexity.

4 Simulation Studies

Numerical simulations were conducted in MATLAB/Simulink to assess the validity of the CIFC approach in force/position tracking and robustness when applied to curved and complex surfaces. The proposed CIFC controller operated at a sampling period of $T = 2\,\text{ms}$, corresponding to a control frequency of 1 kHz. Using an adaptive time-stepping method and the ODE45 solver, the simulations achieved high accuracy and stability. The simulation block diagram is presented in Fig. 4, and the key impedance parameters used in the model are listed in Table 1.

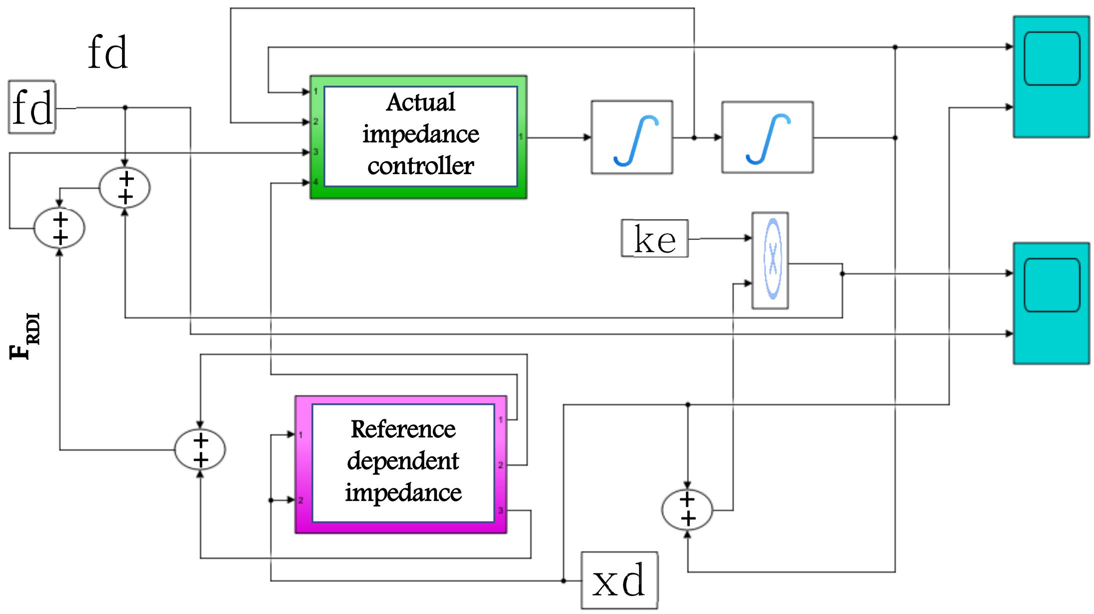

Figure 4: CIFC simulation block diagram.

Table 1: CIFC parameters used for simulation studies.

Case	f_d (N)	k_r (N/m)	b_r (N·s/m)	m_r (kg)	k_e (N/m)
(1)	20	1	20	1	5000
(2)	20	5	30	1	5000
(3)	20	10	40	1	5000

4.1 Simulation Results and Discussion

The results demonstrate that the CIFC framework achieves accurate position and contact force tracking on both curved and complex surfaces.

For the conventional single impedance control strategy, Fig. 5a,b presents the position and force responses on a curved surface, respectively. The CIFC-based position and force tracking results are given in Fig. 5c,d. To improve tracking performance, the proposed CIFC method introduces dynamic impedance reference adjustment through the F_{RDI} compensation signal. For the curved surface case, the force tracking error single impedance, CIFC-based force tracking error, and F_{RDI}-compensated force response are presented in Fig. 6a,c, respectively. A similar evaluation for the complex surface is provided in Fig. 7a,b, while the CIFC-based tracking results are presented in Fig. 7c,d. Furthermore, the evaluation for the complex surface is provided in Fig. 8a–c, confirming consistent performance improvement using the proposed compensation strategy. The F_{RDI} signals in both cases are used to compensate the force errors generated by the single impedance controller and drive them toward zero.

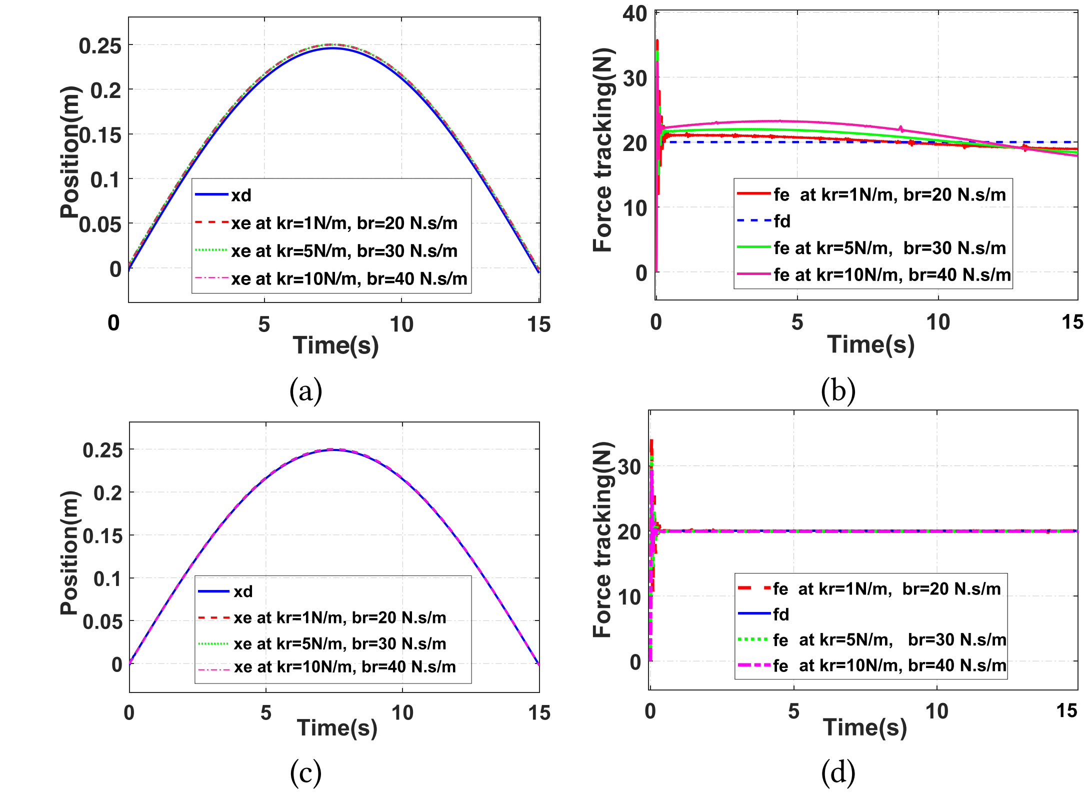

Figure 5: Tracking performance of single impedance control and F_{RDI} compensation on a curved surface: (**a**) position tracking of single impedance control under three stiffness damping combinations; (**b**) force tracking of single impedance control under the same parameter settings; (**c**) position tracking using CIFC impedance control; and (**d**) force tracking using CIFC impedance control.

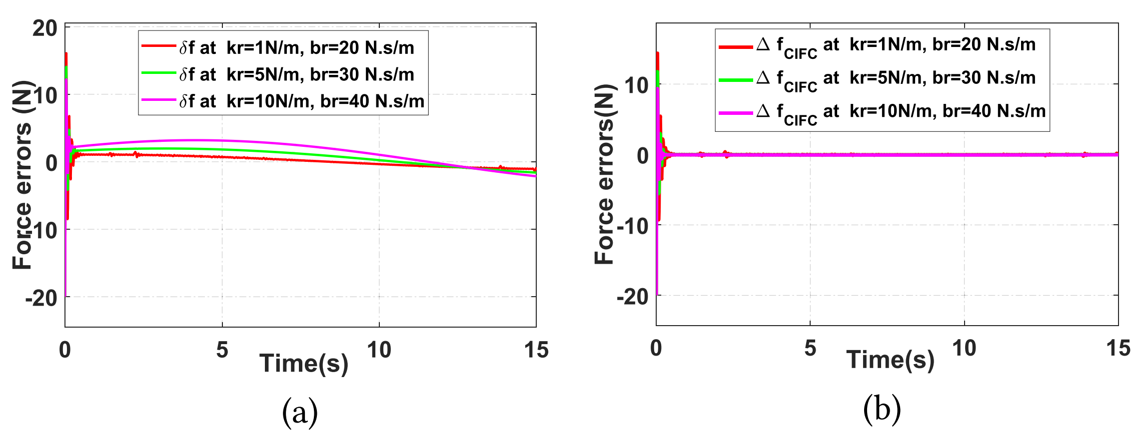

Figure 6: (Continued)

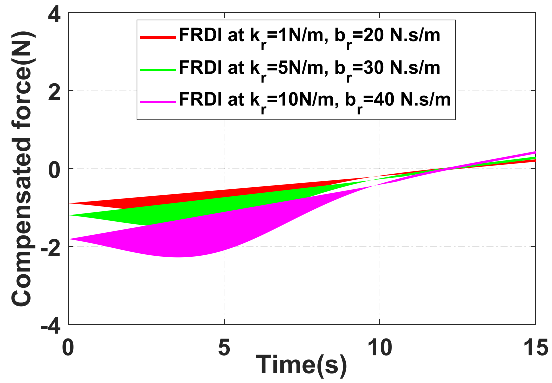

(c)

Figure 6: Performance evaluation of the CIFC controller with F_{RDI} on a curved surface: (**a**) single impedance force tracking under three different combinations of robot stiffness and damping parameters; (**b**) force tracking errors based on CIFC methods; and (**c**) F_{RDI}-compensated force of the proposed method.

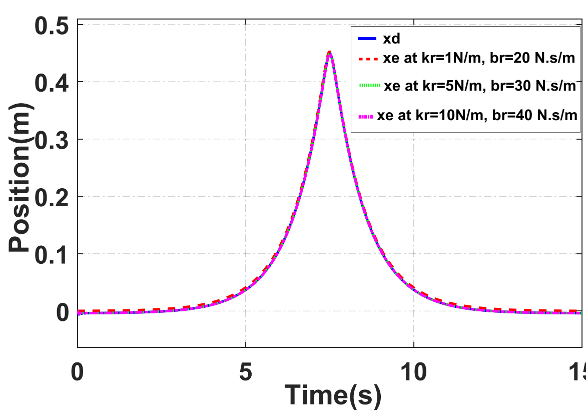

(a)

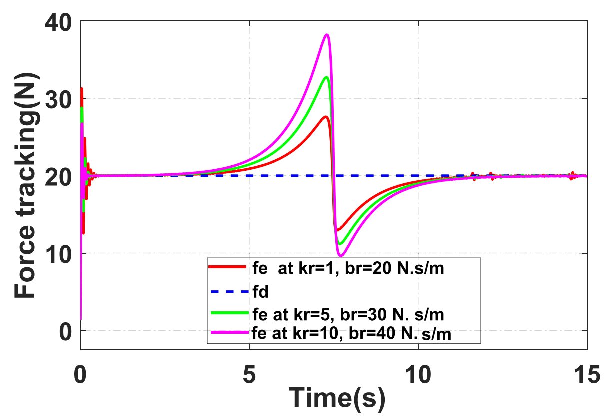

(b)

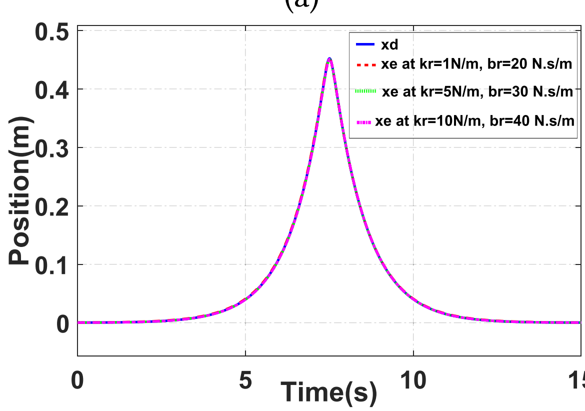

(c)

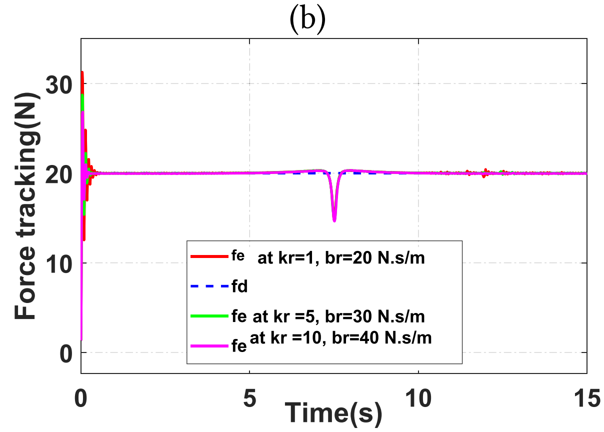

(d)

Figure 7: Single impedance and CIFC-based control performance with F_{RDI} compensation on a complex surface. (**a**) Position behavior under three stiffness damping combinations using single impedance control; (**b**) corresponding force response; (**c**) CIFC position tracking results; and (**d**) CIFC force tracking results.

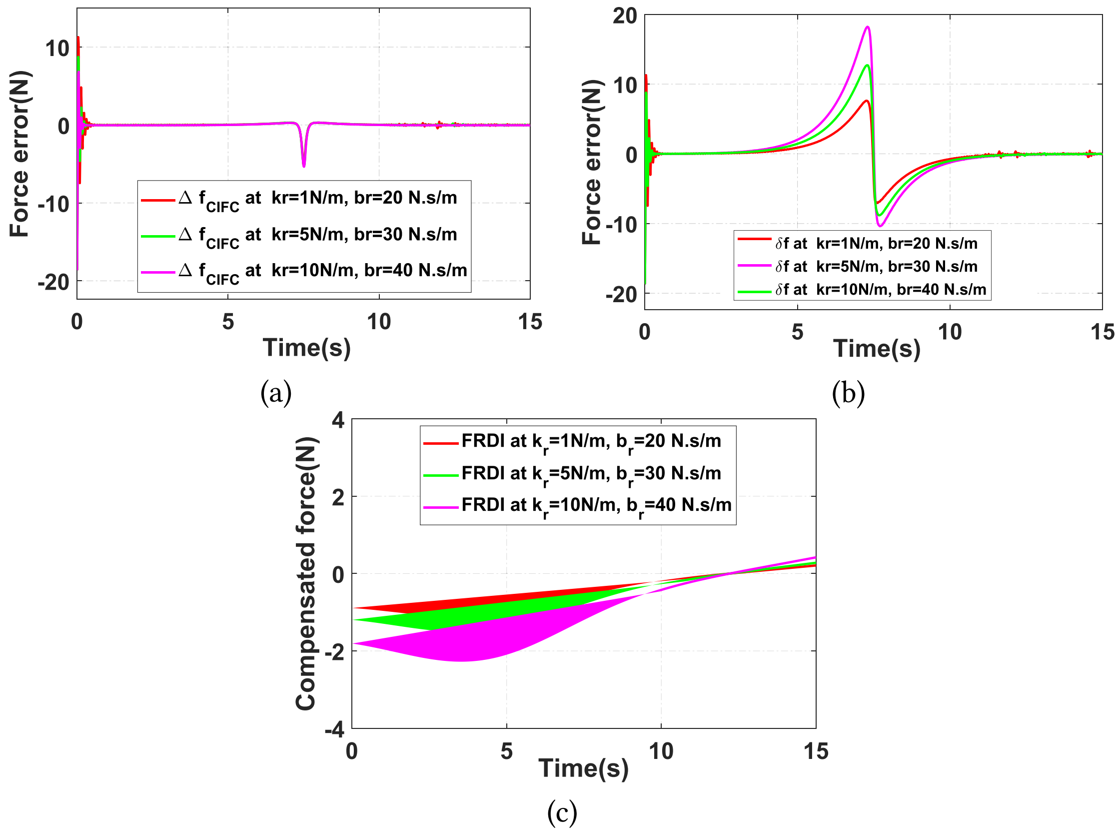

Figure 8: Performance evaluation of the CIFC controller with F_{RDI} on a complex surface: (**a**) single impedance force tracking under three different combinations of robot stiffness and damping parameters; (**b**) force tracking errors using the CIFC method; and (**c**) F_{RDI}-compensated force of the proposed method.

Finally, Fig. 9a,b presents the RMS force tracking errors for the curved and complex surfaces, respectively. The results indicate that the average force error remains approximately 0.15 N in both cases, demonstrating the high tracking accuracy and robustness of the proposed controller.

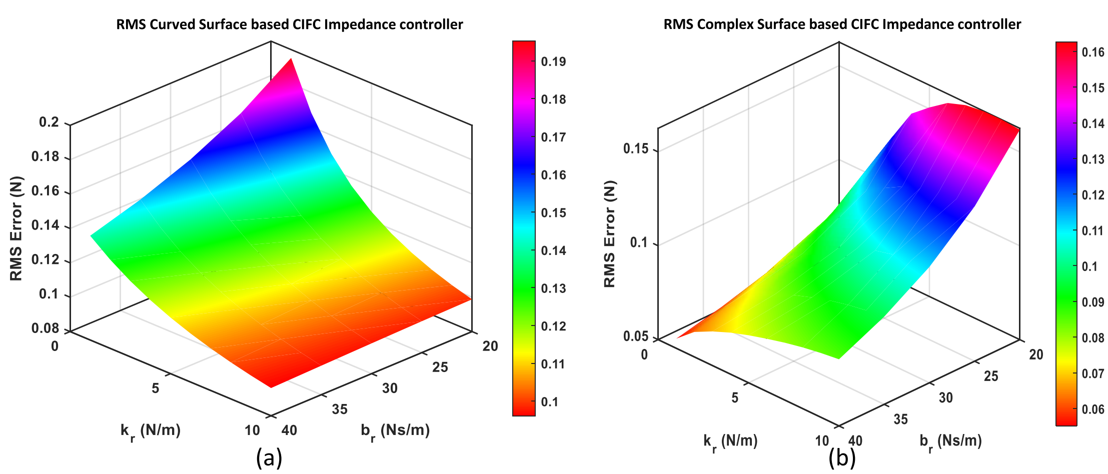

Figure 9: RMS force tracking errors for the CIFC–impedance controller across (**a**) curved surface profile, (**b**) complex surface, demonstrating enhanced force tracking accuracy and regulation.

These findings emphasize the crucial role of the CIFC control method in achieving effective position and force tracking. By dynamically adjusting the interaction force through F_{RDI} compensation signal, the proposed method significantly improves tracking accuracy and minimizes force deviations. The CIFC strategy ensures stable and precise contact interactions, making it particularly suitable for applications requiring accurate contact force control. In contrast to traditional single control techniques, which often struggle to adapt to complex or curved surface geometries, the CIFC method offers a more reliable solution.

In summary, the simulation results highlight the promising capability of the CIFC algorithm, integrated with the F_{RDI} compensation signal, to improve efficiency in contact-based robotic tasks. These positive outcomes establish a strong foundation for experimental validation and real-time implementation, underscoring the approach's potential for advanced force control in robotic systems.

4.2 Simulation Robustness Testing under Multi-Factor Uncertain Conditions

To address the limitation of simplified simulation scenarios, an extended robustness validation was conducted under more realistic and uncertain operating conditions. In addition to the nominal underdamped reference motion, several uncertainty factors were introduced, including measurement noise, sensor disturbances, friction, and variations in drift effects, as summarized in Table 2.

Table 2: Key parameters used in CIFC robustness simulation.

Category	Parameter	Value/Description
Simulation Setup	Sampling time dt	0.01 s
	Simulation time T	30 s
	Random seed	10
Reference Model	Position type	Underdamped sinusoidal
	Amplitude A	0.5 m
	Damping ratio ζ	0.15
	Natural frequency ω_n	1.8 rad/s
Force Reference	Desired force F_d	−5 N
Disturbance Model	Type	Underdamped sinusoidal disturbance
	Amplitude	0.6
	Frequency	0.6 rad/s
	Damping ratio	0.25
Noise and Uncertainty	Measurement noise (Single)	0.03 (std)
	Measurement noise (CIFC)	0.015 (std)
	Drift effect	First order random walk
	Friction effect	Low frequency perturbation
	Sensor disturbance	Additive Gaussian noise

These conditions collectively represent typical challenges in robotic contact tasks with time-varying and uncertain environments. Under these scenarios, the single impedance controller exhibits degraded tracking performance due to limited disturbance rejection capability and parameter sensitivity. In contrast, the proposed CIFC method maintains stable position and force tracking by effectively suppressing external disturbances and modeling uncertainties.

The adaptive compensation mechanism further enhances robustness by mitigating disturbance effects in real time, while the CIFC structure improves tracking accuracy through dynamic error correction and improved force-position coupling control.

Fig. 10a presents the position tracking performance under the proposed CIFC controller and the conventional single impedance controller in the presence of underdamped reference motion and multi-source uncertainties. It can be observed that the proposed method closely follows the desired trajectory with minimal oscillations and faster convergence, while the single impedance controller exhibits noticeable tracking deviations and residual oscillations due to its limited disturbance rejection capability.

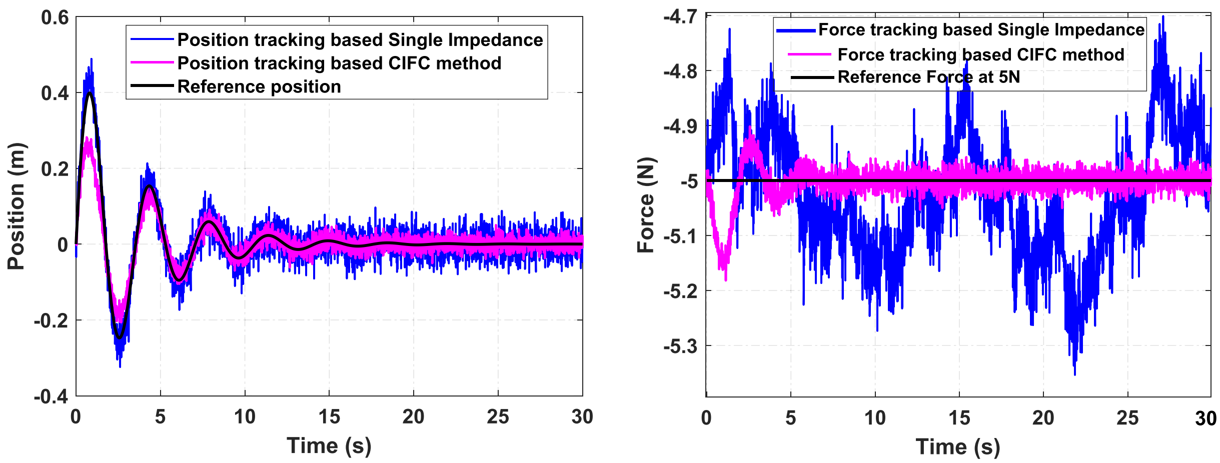

(a) (b)

Figure 10: (**a**) Position tracking performance and (**b**) force tracking performance comparison between the conventional single impedance controller and the proposed CIFC method under underdamped reference motion and multi-source uncertainties.

Fig. 10b illustrates the corresponding force tracking performance under the same conditions. The CIFC controller maintains stable force regulation around the reference value with significantly reduced fluctuations. In contrast, the conventional method shows larger tracking errors and slower recovery from disturbances. These results clearly demonstrate the superior robustness and accuracy of the proposed approach in both position and force control tasks under uncertain and dynamic environments.

4.3 Comparison Study

Over the years, numerous research efforts have introduced strategies aimed at maintaining accurate contact force control in simulation environments. In this section, the performance of two representative methods [5,32] is compared with the CIFC controller. This study evaluates an adaptive variable impedance controller [5] and the Wavelet Neural Network (WNN)-based impedance control algorithm [32] in a ramp surface case in position and force regulation, comparing their performance with the proposed CIFC method.

To ensure consistency across evaluations, all three control strategies were simulated under identical conditions, including a uniform stiffness setting of 5000 N/m and a desired contact force of 50 N. However, each method utilized distinct impedance parameters tailored to its specific control approach. For the CIFC, the impedance parameters applied to the ramp surface were: k_r = 1 N/m, b_r = 40 N·s/m, m_r = 1 kg. For the adaptive variable impedance model, k_r = 0, m_r = 1 kg, where b_r was adjusted online. For the WNN method, k_1 = 0.1 N/m, k_2 = 25 N/m, while the remaining parameters were computed using a WNN controller.

For the adaptive impedance controller [5], the parameters were tuned using a standard trial-and-error procedure. The inertia term was selected based on approximate robot dynamics, while the damping coefficient was gradually increased from conservative values until stable force tracking without oscillation was achieved. The stiffness term was fixed or reduced depending on the adaptation strategy, and the adaptation gain was empirically adjusted to balance response speed and stability. This method requires careful manual tuning of multiple coupled parameters, and its performance is sensitive to these selections. In addition, the computational complexity and implementation requirements are relatively higher due to online parameter adaptation.

For the WNN-based impedance controller reported in [32], a two-layer structure combining impedance control with a Wavelet Neural Network was implemented. The network configuration (number of hidden nodes and wavelet basis functions) and learning rates were selected empirically. The learning process requires sequential tuning, starting from a stabilized impedance controller and gradually activating adaptation. Performance is influenced by learning rate selection and may degrade if tuning is not carefully balanced between convergence speed and stability. Moreover, the computational complexity and implementation requirements are increased due to real-time neural network training and weight updating.

In contrast, the proposed CIFC method uses a fixed parameter structure based on F_{RDI} formulation, requiring only a small number of physically interpretable gains. The damping term plays the dominant role in ensuring stability and is tuned in a straightforward manner, while inertia and stiffness are selected based on nominal system behavior. Unlike adaptive and learning-based approaches, CIFC does not require iterative learning, weight tuning, or parameter scheduling, which significantly improves reproducibility and reduces implementation complexity. Importantly, the same parameter set is consistently used across all simulation scenarios without retuning, demonstrating the robustness and effectiveness of the proposed controller. The experimental validation is conducted using the controller parameters from Case (3) with $k_r = 10$ and $b_r = 30$. Furthermore, the computational complexity and implementation requirements are relatively low due to the absence of online adaptation or learning mechanisms.

The comparison illustrated in Figs. 11 and 12 indicate that, while WNN-based and adaptive impedance control strategies outperform traditional single impedance techniques, they still exhibit notable limitations in terms of force tracking accuracy and transient response. Although the WNN-enhanced controller attains satisfactory results, this occurs only after a period of network adaptation; in contrast, the adaptive impedance strategy improves gradually through continuous tuning of parameters. Finally, Fig. 13a,b illustrates the RMS force errors generated by the proposed method for the two surfaces, respectively. In addition the results indicate that the proposed CIFC controller achieves RMS force errors of approximately 1.9 N during the transient period (0–1 s) and 0.15 N during the steady state period (1–3 s) as summarized in Table 3. Which demonstrating its high force tracking accuracy and effective disturbance rejection capability.

By contrast, the proposed CIFC scheme consistently delivers superior force tracking, achieving minimal position error with rapid response times. This enhanced performance is attributed to its real-time compensation of the force reference-dependent impedance parameter. These results confirm that the proposed system is highly suitable for applications involving accurate force tracking.

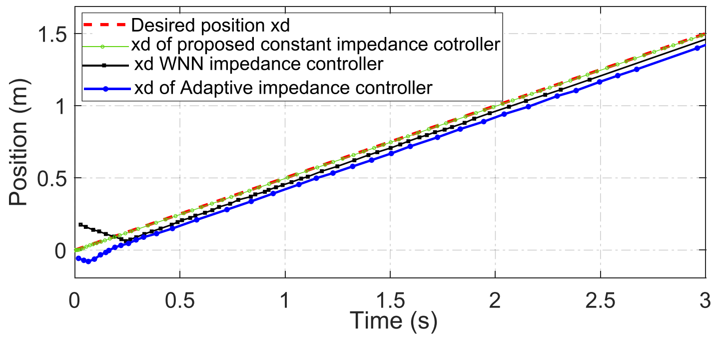

Figure 11: Position tracking using the proposed constant impedance controller compared to WNN-impedance and adaptive impedance controllers.

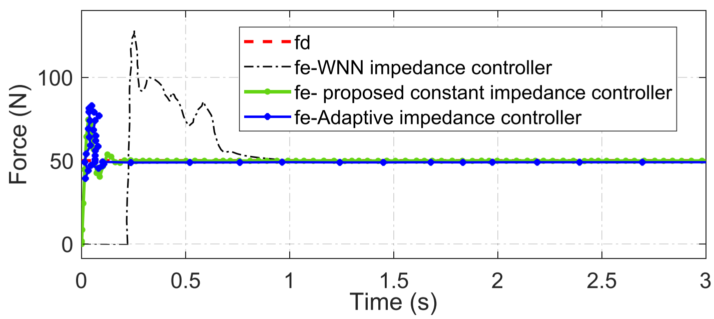

Figure 12: Force tracking using the proposed constant impedance controller compared to WNN-impedance and adaptive impedance controllers.

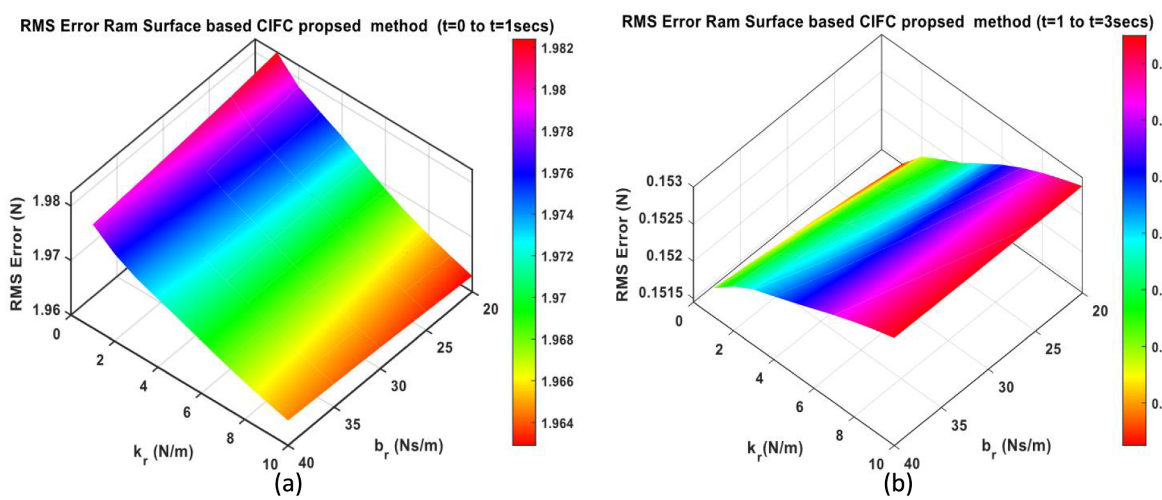

Figure 13: RMS force tracking errors for the impedance-CIFC controller across the RAMP surface (**a**) case1 (t = 0–1) s; (**b**) case2 (t = 1–3) s, demonstrating enhanced force-tracking accuracy.

Table 3: Comparison of RMS force tracking error, peak force, settling time, and overall performance for adaptive impedance, WNN-based impedance, and CIFC–Impedance controllers.

Controller	Peak Error (N)	RMS (N) at (0–1) s	RMS (N) at (1–3) s	Performance
WNN Impedance Controller	130	20.1	0.64	Large overshoot and oscillation
Adaptive Impedance Controller	80	3.2	0.32	Moderate tracking accuracy
CIFC impedance controller	60	1.9	0.15	Best tracking performance

5 Experimental Studies

This section presents experimental validation on curves and complex surfaces, closely aligned with simulation studies to ensure strong validation.

5.1 Experimental Setup

The experimental setup is shown in Figs. 14 and 15. A UR10 robotic manipulator is equipped with a six-axis force/torque sensor (ATI Gamma) mounted between the robot flange and a pneumatic polishing tool of approximately 1.0 kg mass. The force/torque sensor is calibrated using a manufacturer-provided zero-offset procedure before each trial.

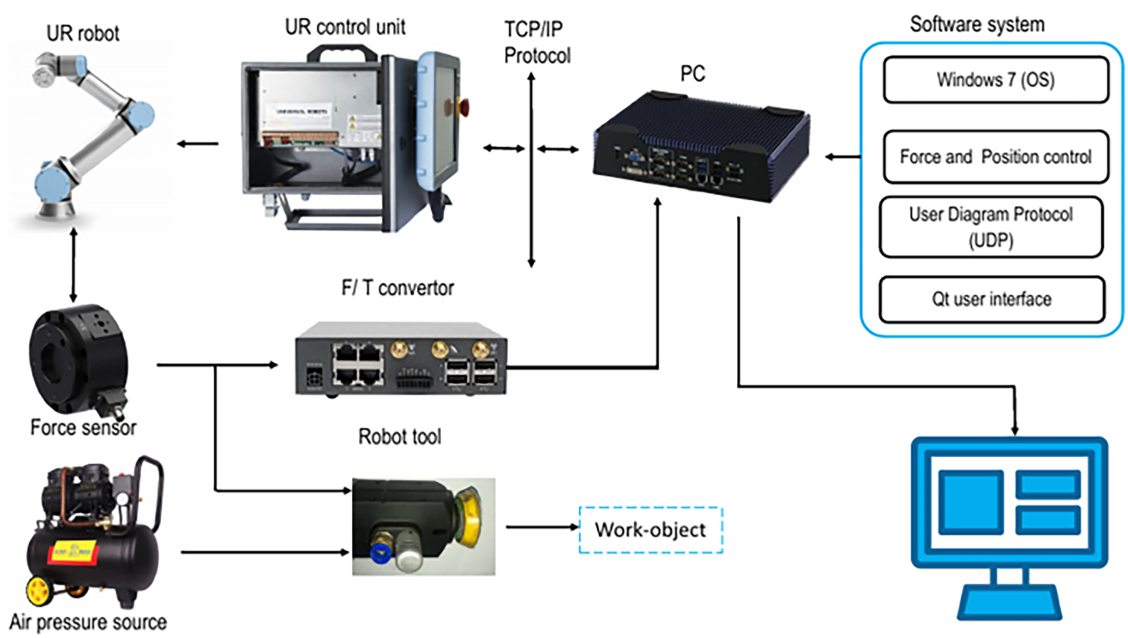

Figure 14: Experimental setup.

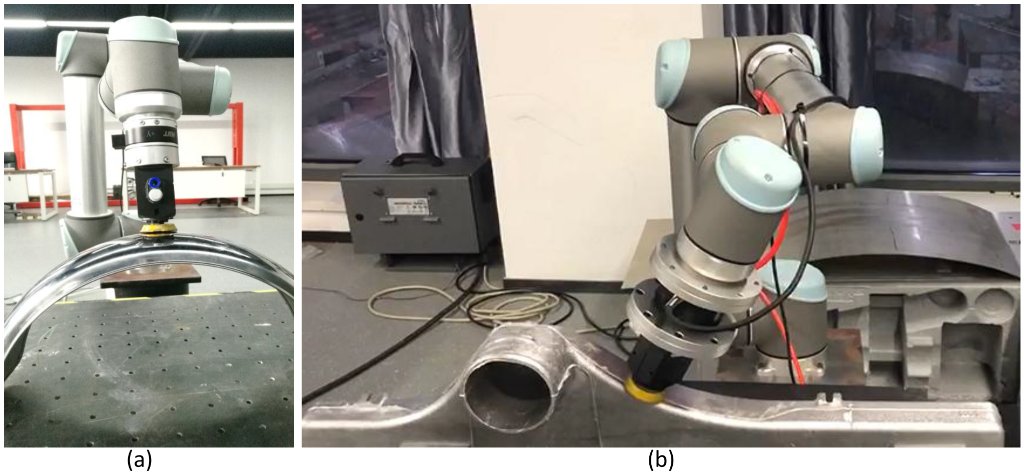

Figure 15: Robotic contact process setup on (a) curved and (b) complex surfaces.

The workpiece is an aluminum specimen of a curved surface (D = 100 mm, circumference = 314 mm) and a complex ramp with an irregular shape. The real-time control system operates at 500 Hz (2 ms sampling period), with synchronized acquisition of force and position signals.

Communication between the industrial PC and the robot controller is implemented via TCP/IP, with a 3–5 ms delay compensated using buffering. Safety is ensured using the built-in joint limits of the UR10 and an emergency stop condition triggered when the contact force exceeds 30 N.

5.2 Implementation Details

The proposed CIFC controller was implemented in C++ on an industrial PC and integrated with a UR10 robotic manipulator through a TCP/IP communication interface. The control architecture consists of an outer CIFC force-position controller and the manufacturer's built-in inner joint position controller. Force and position measurements were acquired in real time and synchronized with the control loop, ensuring full-time alignment with the controller execution cycle. The sampling time of the control system was fixed at 2 ms (500 Hz), and both force and position feedback signals were updated at the same frequency using synchronized data acquisition. These synchronized measurements were used to generate corrective control commands for the contact task. The controller gains and implementation parameters were selected experimentally to ensure stable force tracking and smooth motion during polishing operations.

The key implementation and controller parameters used in the experiments are summarized in Table 4. Consistent with our simulation studies, the polishing-like task was performed on curved and complex surfaces that closely resemble those analyzed in the simulated environment. These surface geometries are shown in Fig. 15.

5.3 Experimental Results and Analysis

The proposed CIFC method demonstrated superior performance in both position and force tracking on curved and complex surfaces.

Table 4: Real-time implementation parameters of the CIFC controller.

Parameter	Value/Description
Robot platform	UR10 manipulator
Control software	C++
Communication	TCP/IP
Outer-loop controller	Proposed CIFC controller
Inner-loop controller	UR10 built-in joint position controller
Sampling time	2 ms
Control frequency	500 Hz
Force feedback rate	500 Hz
Position feedback rate	500 Hz
Force sensor	ATI Gamma 6-axis Force/Torque sensor
Signal filtering	First-order low-pass filter (20 Hz cutoff frequency)
m_r	1 kg
b_r	40 N·s/m
k_r	10 N/m
k_e	5000 N/m
Tool speed	3000–4000 rpm
Contact force	10 N
Pneumatic pressure	0–10 bar
Abrasive grit size	P600

The experimental results for curved and complex surface finishing are presented in Figs. 16–19 to evaluate the performance of the proposed CIFC control method. For the curved surface case, the position tracking comparison between the traditional impedance controller and the proposed CIFC controller is shown in Fig. 16. The robot successfully follows the desired curved trajectory, while the proposed controller provides smoother motion with reduced tracking deviation. The corresponding force tracking performance under different desired contact forces (5, 10, and 15 N) is illustrated in Fig. 17. The proposed CIFC controller achieves stable contact force regulation with smaller fluctuations, demonstrating improved adaptability to different force levels compared with the traditional impedance controller.

For the complex surface experiment, the position tracking results are shown in Fig. 18. Compared with the curved surface case, the increased geometric variation introduces more challenging motion requirements. The proposed CIFC method maintains accurate trajectory tracking and provides better compensation against surface disturbances. Furthermore, the force tracking results for different reference forces (5, 10, and 15 N) are presented in Fig. 19. The proposed controller maintains consistent force tracking performance over the tested force range, while the conventional impedance controller exhibits larger tracking errors and force oscillations. These results verify that the proposed CIFC strategy improves both trajectory following and contact force regulation during robotic finishing processes on complex surfaces.

Overall, the developed CIFC strategy with the effect of F_{RDI} compensation signal demonstrated accurate position tracking and consistent force regulation across both simulated and experimental polishing scenarios. It significantly improves the robot's capability to control motion and force while adapting to dynamic, curved, and complex surfaces. By ensuring stable force application and precise position tracking, this approach enables reliable execution of complex tasks, making it particularly well suited for high-precision applications requiring sustained physical contact.

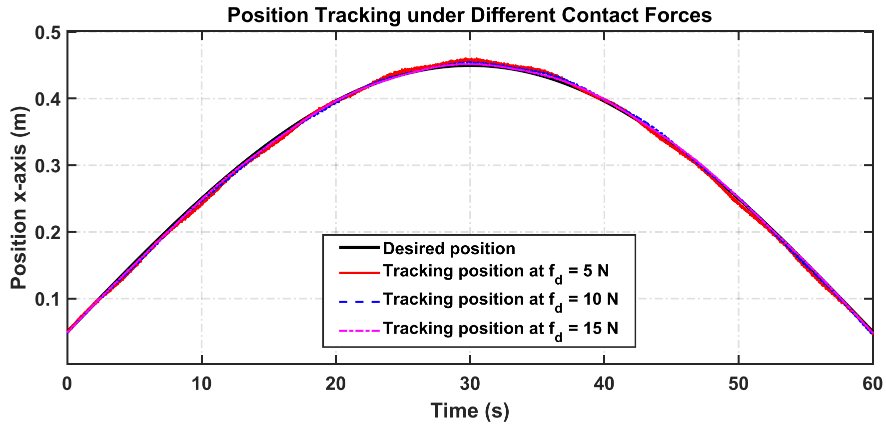

Figure 16: Position tracking on a curved surface as a comparison between the traditional impedance controller and the proposed CIFC control method.

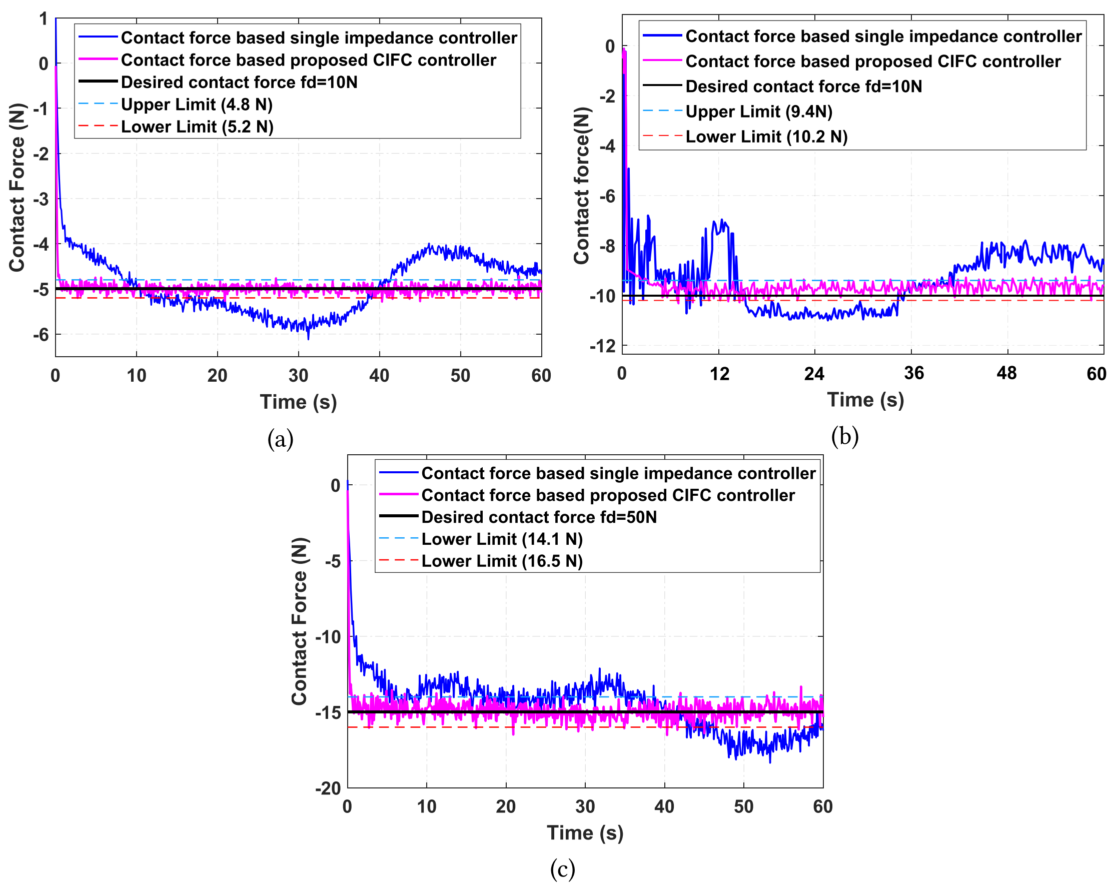

Figure 17: Comparative real-time force tracking performance on a curved surface under varying reference forces between the conventional single impedance control and the proposed CIFC-based control strategy: (**a**) 5 N reference force, (**b**) 10 N reference force, and (**c**) 15 N reference force.

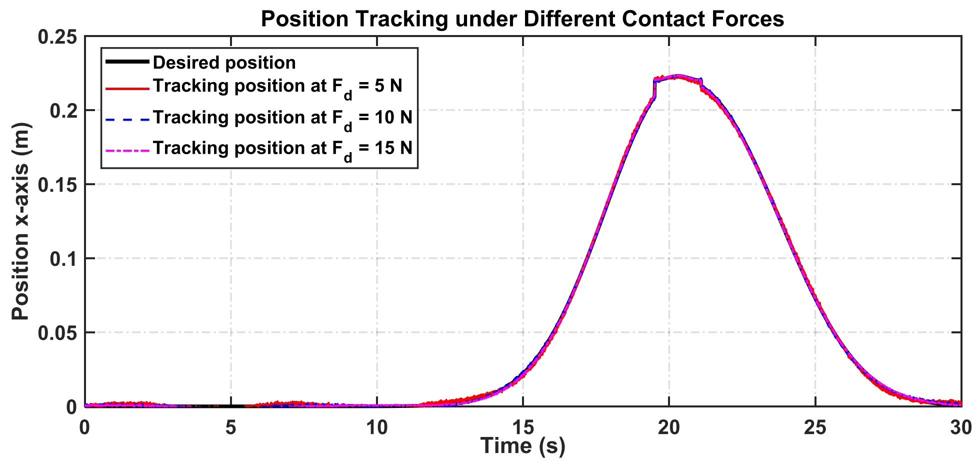

Figure 18: Position tracking of a complex surface as a comparison between traditional single impedance controller and proposed CIFC control method.

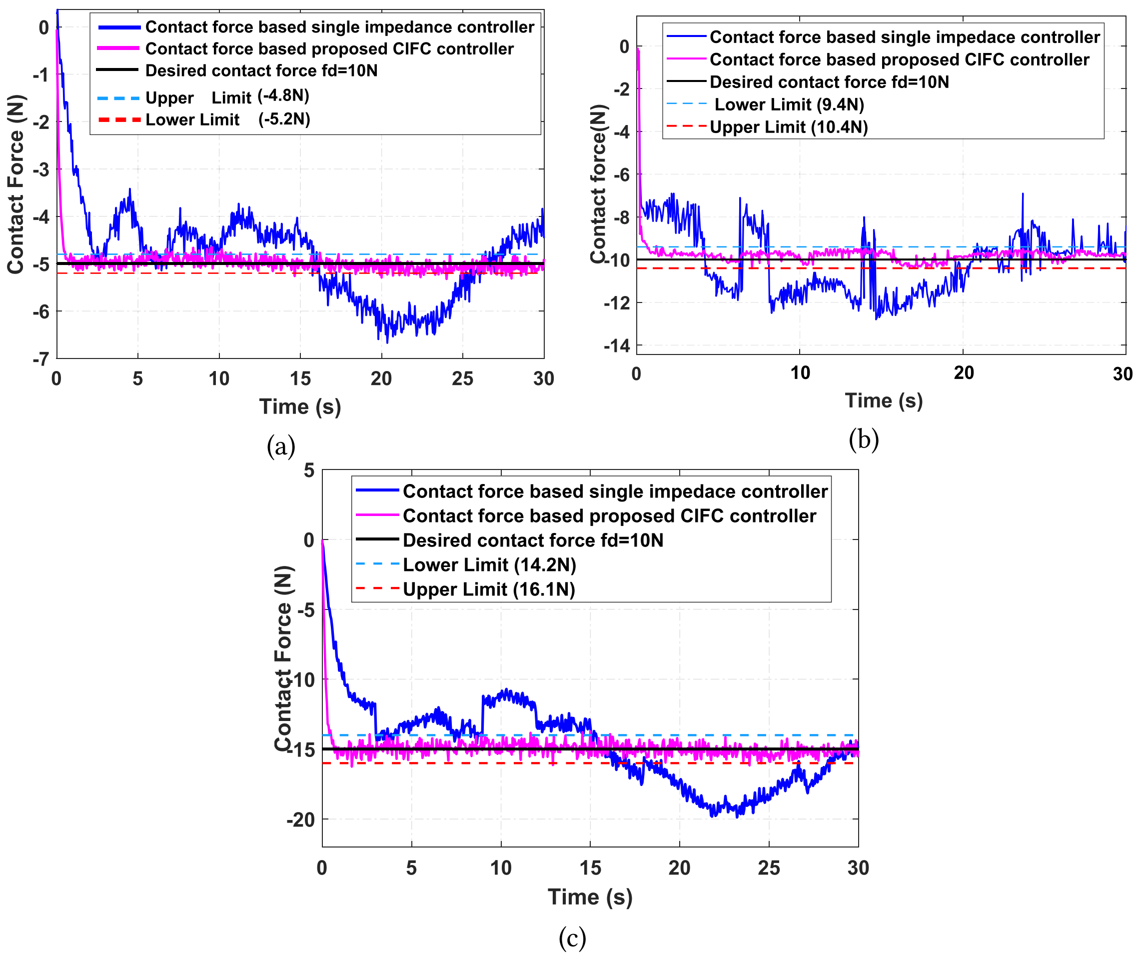

Figure 19: Comparative real-time force tracking performance on a complex surface under varying reference forces between the conventional single impedance control and the proposed CIFC- based control strategy: (**a**) 5 N reference force, (**b**) 10 N reference force, and (**c**) 15 N reference force.

The RMS, MAE, and standard deviation (STD) of the force tracking errors for both the traditional single impedance controller and the proposed CIFC method under different reference forces are summarized in Table 5. The results indicate that the proposed CIFC approach consistently achieves lower RMS, MAE, and STD values across all tested force levels (5, 10, and 15 N) compared with the conventional impedance controller. This demonstrates that the proposed method not only improves overall tracking accuracy but also enhances consistency and stability in force regulation. In addition, the improvement percentage clearly highlights the superiority of the CIFC strategy, particularly at higher reference forces, where more significant reductions in tracking errors are observed. These results confirm the strong robustness and scalability of the proposed controller for robotic surface interaction tasks.

Table 5: Statistical performance comparison between single impedance control and CIFC controller under different reference forces.

Force (N)	Method	RMS (N)	MAE (N)	Std (N)	Improvement (%)
5	Single Impedance	1.78	1.42	0.65	86.5
5	CIFC controller	0.24	0.18	0.08	—
10	Single Impedance	2.12	1.70	0.78	82.6
10	CIFC controller	0.37	0.29	0.12	—
15	Single Impedance	3.88	3.10	1.25	86.6
15	CIFC controller	0.52	0.41	0.16	—

6 Conclusions

This paper presents a Constant Impedance Force Control (CIFC) framework for robotic contact-based tasks. The proposed approach integrates a Force Reference Dependent Impedance (F_{RDI}) compensation mechanism within the classical impedance control framework while maintaining fixed impedance parameters. The proposed method enhances contact force regulation by compensating force deviations according to the desired interaction force and contact conditions.

Comprehensive validation through simulation, comparative analysis, and real-time experiments demonstrates that the proposed CIFC framework achieves accurate force tracking and stable position regulation under different surface conditions. The results show that the proposed compensation mechanism improves adaptability during interaction with curved and complex geometries, providing an effective and computationally efficient solution for contact-based manufacturing applications such as polishing.

Although the proposed CIFC framework demonstrates promising performance, some limitations remain. The stability analysis is based on a reduced-order contact model, and the experimental validation is conducted on representative surface interaction tasks such as polishing processes. Further studies considering full robot dynamics and broader contact scenarios such as grinding, deburring, and similar operations are required to further evaluate and enhance its generality and robustness.

Future work will focus on extending the CIFC framework toward variable force control strategies and conducting more comprehensive experimental investigations under diverse industrial contact scenarios, including varying material properties, external disturbances, and a wider force range, to further enhance robustness and practical applicability. In addition, the proposed method will be extended to more complex operations such as grinding, deburring, cutting, and similar manufacturing tasks, alongside the exploration of AI-based approaches to improve adaptability and performance in highly uncertain environments.

Acknowledgement: The authors would like to thank Prof. Dr. Ali Ahmed Alfakiabdalla (King Abdulaziz University, Saudi Arabia) and Dr. Yang Yang (Research Institute of China Electronics Technology Group Corporation (CETC), China) for their valuable comments and support.

Funding Statement: This work was supported by the Fujian Provincial Natural Science Foundation of China (Grant No. 2026J0012053); and the Fujian Provincial Project for Young and Middle-aged Researchers (Grant No. JAT251214).

Author Contributions: The following list outlines the authors' contributions to this paper: conceptualization, writing—original draft preparation, Abubaker Ahmed; validation, supervision, Hosham Wahballa; software, Arafat Abdulgader Mohammed Elhag, Ahmed Hamza Osman; formal analysis, Ala Eldin Awouda, Arafat Abdulgader Mohammed Elhag, Ahmed Hamza Osman; writing—review and editing, Hosham Wahballa, Ala Eldin Awouda, Abubaker Ahmed; visualization, Mubarak Himmat, Arafat Abdulgader Mohammed Elhag; funding acquisition by Hosham Wahballa, Ala Eldin Awouda. All authors reviewed and approved the final version of the manuscript.

Availability of Data and Materials: Data are contained within the article.

Ethics Approval: Not applicable.

Conflicts of Interest: The authors declare no conflict of interest.

References

1. Hogan N. Impedance control: an approach to manipulation: Part II implementation. ASME J Dyn Sys Meas Control. 1985 Mar;107(1):816. doi:10.1115/1.3140713.
2. Yun W, Choi K, Kim J, Oh S, Chung H. Low impedance rendering toward safe human-robot interaction. In: Proceedings of the ACM/IEEE International Conference on Human-Robot Interaction; 2025 Mar 4–6; Melbourne, Australia. p. 1750–3. doi:10.1109/HRI61500.2025.10974040.
3. Averta G, Hogan N. Enhancing robot-environment physical interaction via optimal impedance profiles. In: Proceedings of the IEEE 8th RAS/EMBS International Conference on Biomedical Robotics and Biomechatronics; 2020 Nov 29–Dec 1; New York, NY, USA. p. 973–80. doi:10.1109/BioRob49111.2020.9224382.
4. Wahballa H, Gibreel M, Ahmed A, Chen X, Weining L. Precise contact tracking on complex geometries using polishing machine tools via smooth trajectories within online constant force control. Eng Sci Technol Int J. 2025;72(8):102226. doi:10.1016/j.jestch.2025.102226.
5. Duan J, Gan Y, Chen M, Dai X. Adaptive variable impedance control for dynamic contact force tracking in uncertain environment. Robot Auton Syst. 2018;102(1):54–65. doi:10.1016/j.robot.2018.01.009.
6. Ding RQ, Wang JH, Cheng M, Sun MK, Xu B, Wang Z. Adaptive impedance control for the hydraulic manipulator under the uncertain environment. J Braz Soc Mech Sci Eng. 2023;45(8):437. doi:10.1007/s40430-023-04323-6.
7. Song P, Yu Y, Zhang X. A tutorial survey and comparison of impedance control on robotic manipulation. Robotica. 2019;37(5):801–36. doi:10.1017/S0263574718001339.
8. Jung S, Hsia TC, Bonitz RG. Force tracking impedance control of robot manipulators under unknown environment. IEEE Trans Control Syst Technol. 2004;12(3):474–83. doi:10.1109/TCST.2004.824320.
9. Cao H, He Y, Chen X, Zhao X. Smooth adaptive hybrid impedance control for robotic contact force tracking in dynamic environments. Ind Robot. 2020;47(2):231–42. doi:10.1108/IR-09-2019-0191.
10. Siciliano B, Sciavicco L, Villani L, Oriolo G. Robotics: modelling, planning and control. London, UK: Springer; 2009. 10.1007/978-1-84628-642-1-10.
11. Spong MW, Hutchinson S, Vidyasagar M. Robot modeling and control, vol. 2. New York, NY, USA: Wiley; 2020. 10.1109/MCS.2021.3122271.
12. Wang G, Deng Y, Zhou H, Yue X. PD-adaptive variable impedance constant force control of macro-mini robot for compliant grinding and polishing. Int J Adv Manuf Technol. 2023;124:2149–70. doi:10.1007/s00170-022-10405-x.
13. Wang X, Li C, Cai D, Cui Y. Research on adaptive variable impedance control method based on adaptive neuro-fuzzy inference system. Sensors. 2025;25(10):3055. doi:10.3390/s25103055.

14. Ge D, Zhao H, Wang Y, Li D, Li X, Ding H. Learning compliant dynamical system from human demonstrations for stable force control in unknown environments. Robot Comput Integr Manuf. 2024;86(3):102669. doi:10.1016/j.rcim.2023.102669.
15. Tang S, Chai Z, Wang X, Chang H, Guo X. Adaptive impedance control method for manipulator based on radial basis function. Ind Robot. 2025;52(2):238–48. doi:10.1108/IR-07-2024-0327.
16. Liang J, Zhong H, Wang Y, Chen Y, Zeng J, Mao J. Adaptive force tracking impedance control for aerial interaction in uncertain contact environment using barrier function. IEEE Trans Autom Sci Eng. 2023;21(3):4720–31. doi:10.1109/TASE.2023.3301023.
17. Iskandar M, Ott C, Albu-Schffer A, Siciliano B, Dietrich A. Hybrid force-impedance control for fast end-effector motions. IEEE Robot Autom Lett. 2023;8(7):3931–8. doi:10.1109/LRA.2023.3270036.
18. Xu Z, Li S, Zhou X, Zhou S, Cheng T, Guan Y. Dynamic neural networks for motion-force control of redundant manipulators: an optimization perspective. IEEE Trans Ind Electron. 2020;68(2):1525–36. doi:10.1109/TIE.2020.2970635.
19. Peng J, Ding S, Yang Z, Xin J. Adaptive neural impedance control for electrically driven robotic systems based on a neuro-adaptive observer. Nonlinear Dyn. 2020;100(2):1359–78. doi:10.1007/s11071-020-05569-8.
20. Naceri A, Schumacher T, Li Q, Calinon S, Ritter H. Learning optimal impedance control during complex 3D arm movements. IEEE Robot Autom Lett. 2021;6(2):1248–55. doi:10.1109/LRA.2021.3056371.
21. Sharifi M, Azimi V, Mushahwar VK, Tavakoli M. Impedance learning-based adaptive control for human-robot interaction. IEEE Trans Control Syst Technol. 2021;30(4):1345–58. doi:10.1109/TCST.2021.3107483.
22. Shahriari E, Birjandi SAB, Haddadin S. Passivity-based adaptive force-impedance control for modular multi-manual object manipulation. IEEE Robot Autom Lett. 2022;7(2):2194–2201. doi:10.1109/LRA.2022.3142903.
23. Saat S, Ahmad MA, Tumari MZM, Suid MH, Ghazali MR. Optimal brain emotional learning with PID control for flexible joint manipulators. Appl Modell Simul. 2026;10:11–27.
24. Kasruddin Nasir AN, Ahmad MA, Tokhi MO. Hybrid spiral-bacterial foraging algorithm for a fuzzy control design of a flexible manipulator. J Low Freq Noise Vib Act Control. 2022;41(1):340–58. doi:10.1177/14613484211035646.
25. Ghazali MRB, Ahmad MAB, Raja Ismail RMTB. Adaptive safe experimentation dynamics for data-driven neuroendocrine-PID control of MIMO systems. IETE J Res. 2022;68(3):1611–24. doi:10.1080/03772063.2019.1656556.
26. Ajani OS, Assal SF. Hybrid force tracking impedance control-based autonomous robotic system for tooth brushing assistance of disabled people. IEEE Trans Med Robot Bionics. 2020;2(4):649–60. doi:10.1109/TMRB.2020.3030317.
27. Jung S, Lee JW. Hybrid impedance force tracking control of a robot manipulator under non-model dynamics and nonlinear uncertainties. Asian Control Conf. 2022:1108–13. doi:10.23919/ASCC56756.2022.9828122.
28. Li G, Chen X, Yu J, Liu J. Adaptive neural network-based finite-time impedance control of constrained robotic manipulators with disturbance observer. IEEE Trans Circuits Syst II Express Briefs. 2021;69(3):1412–6. doi:10.1109/TCSII.2021.3109257.
29. Hasanzadeh Fereydooni R, Siahkali H, Shayanfar HA, Mazinan AH. sEMG-based variable impedance control of lower-limb rehabilitation robot using wavelet neural network and model reference adaptive control. Ind Robot. 2020;47(3):349–58. doi:10.1108/IR-10-2019-0210.
30. Roveda L, Maskani J, Franceschi P, Abdi A, Braghin F, Molinari Tosatti L, et al. Model-based reinforcement learning variable impedance control for human-robot collaboration. J Intell Robot Syst. 2020;100(2):417–33. doi:10.1007/s10846-020-01183-3.
31. Ahmed A, Ju H, Yang Y, Wahballa H, Mustafa GIY. A new integrated method to improve the computation of the robotics inverse kinematics in a simple and unified formula. Machines. 2025;13(12):1073. doi:10.3390/machines13121073.
32. Hamedani MH, Sadeghian H, Zekri M, Sheikholeslam F, Keshmiri M. Intelligent impedance control using wavelet neural network for dynamic contact force tracking in unknown varying environments. Control Eng Pract. 2021;113(1):104840. doi:10.1016/j.conengprac.2021.104840.